Apparent horizon finder for a special family of spacetimes in 3D numerical relativity

Masaru Shibata
Department of Earth and Space Science, Graduate School of Science, Osaka University, Toyonaka, Osaka 560, Japan
(Received 17 June 1996)

We present a method to find the apparent horizon (AH) on a special family of three-dimensional (3D) spacelike hypersurfaces which has π-rotation symmetry around the z axis as well as the reflection one with respect to the equatorial plane. In a nonaxisymmetric 3D hypersurface, the AH, if it exists, is determined by solving a 2D elliptic-type equation. In the present method, we solve the elliptic-type equation as a boundary value problem. To test this method, we apply it to a variety of nonaxisymmetric 3D hypersurfaces which can be obtained by solving the constraint equations in general relativity. We find that the present method works well in all cases. [S0556-2821(97)04904-7]

PACS number(s): 04.25.Dm, 04.20.Ha

I. INTRODUCTION

One of the most important issues in numerical relativity is to clarify the formation process of a black hole (BH) because its formation will be a common phenomenon in astrophysical situations. For example, if a stellar core collapses in the final phase of a very massive star, a BH will be produced. Also, the final fate of coalescence of binary neutron stars (BNS's) or BH's will be a BH. These BH formation processes are also the most promising sources of gravitational radiation for planned kilometer size laser interferometric gravitational wave detectors such as the Laser Interferometric Gravitational Wave Observatory (LIGO) [1] and VIRGO [2]. In analyzing the signal of gravitational waves from such objects to extract a variety of information from them, we will need theoretical knowledge on the formation process of BH's. By comparing a theoretical prediction of a signal of gravitational waves with the detected one, we will be able to extract information from the signal. Thus, we need an investigation of the formation process of BHs theoretically, which is possible only by a three-dimensional (3D) fully relativistic simulation.

A BH is characterized by an event horizon (EH) which is defined as the boundary of the causal past of future null infinity [3]. Hence, in order to understand the formation process of a BH, we should investigate the formation and evolution of the EH in numerical relativity. A technique to find the EH has been developed by a few groups [4,5], and they showed successful results in axisymmetric simulations. However, to find the EH in 3D numerical relativity, we need to save a large amount of numerical data in general because of the global nature of the EH in spacetime. Although future computers may have memory to store such a large amount of data sets, that seems very difficult now. Hence, the EH is not a useful notion in 3D numerical relativity.

In contrast with the EH, the apparent horizon (AH) is very useful as an approximate notion of the EH [3], and has often been used in numerical relativity. The AH is defined as the outermost spacelike and closed two-surface such that the expansion of future-directed outgoing null congruence orthogonal to the two-surface vanishes. A useful property of the AH is that it always lies inside the EH in the globally hyperbolic spacetime [3]. Thus, if the AH exists, the existence of the EH, i.e., the formation of a BH, is guaranteed. Furthermore, in contrast with the EH, we have only to retain numerical data sets of a 3D spacelike hypersurface to determine whether or not the AH exists. Hence, we do not have to worry about the computer memories.

In order to determine the two-surface of the AH, $h(\theta,\varphi)$, in 3D numerical relativity, we need to solve a 2D elliptic-type equation with an appropriate boundary condition which is determined from the regularity of the two-surface. Here, the elliptic-type equation is [see Eq. (2.6)]

$$h_{,\theta\theta}+\cot\theta h_{,\theta}+\frac{h_{,\varphi\varphi}}{\sin^2\theta}-2h=S(h,g_{\mu\nu}), \tag{1.1}$$

where $S(h,g_{\mu\nu})$ depends on nonlinear terms in h as well as the geometric variable $g_{\mu\nu}$. To guarantee the regularity everywhere on the two-surface, Nakamura, Oohara, and Kojima [6] proposed a method in which the spherical harmonic expansion is utilized. In their method, they expand h by the spherical harmonic function $Y_{\ell,m}(\theta,\varphi)$ as

$$h(\theta,\varphi)=\sum_{\ell,m} a_{\ell,m}Y_{\ell,m}(\theta,\varphi), \tag{1.2}$$

where $a_{\ell,m}$ is a coefficient. Then, $a_{\ell,m}$ can be written as

$$a_{\ell,m}=-\frac{1}{\ell(\ell+1)+2}\int d(\cos\theta) \times\int d\varphi Y_{\ell,m}(\theta,\varphi)^*S(h,g_{\mu\nu}), \tag{1.3}$$

where $Y^*_{\ell,m}$ denotes the complex conjugate of $Y_{\ell,m}$. Thus, once a trial value of h is given, $a_{\ell,m}$ can be calculated and then the new trial value of h is obtained. If this procedure is repeated up to convergence of $a_{\ell,m}$, the AH is determined. An important point is that the regularity of the two-surface is completely guaranteed because $h(\theta,\varphi)$ is expanded by the regular function $Y_{\ell,m}$. Using this method, they succeeded in determining the AH for several time-symmetric 3D hypersurfaces which are given analytically.

As criticized by Nakao [7], however, this method does not seem to be efficient when we apply it to the numerical data

sets of 3D hypersurfaces because of the nature of $Y_{\ell,m}$: Since $Y_{\ell,m}$ becomes a more and more variable function in the θ coordinate with an increase of ℓ, we need a careful choice of grid points and weight factors to guarantee the orthogonality of $Y_{\ell,m}$ in numerical integral as

$$2\pi\sum_{i=1}^{N_\ell} Y_{\ell,m}(\theta_i,\varphi)Y_{\ell',m}(\theta_i,\varphi)^*\nu_i=\delta_{\ell,\ell'}, \qquad (1.4)$$

where θ_i and ν_i denote the appropriate grid points and weight factors, and N_ℓ is determined by our choice of the largest $\ell(\ell_{\max})$. Here, $|\nu_i|$ in each grid point is required to become larger and larger with an increase of $\ell_{\max}$ to guarantee the orthogonality of $Y_{\ell,m}$ accurately. Numerical calculation of the integral by θ in Eq. (1.3) is performed as

$$\sum_{i=1}^{N_\ell} Y_{\ell,m}(\theta_i,\varphi)^*S(h,g_{\mu\nu})\nu_i. \qquad (1.5)$$

If a small truncation error is included in $g_{\mu\nu}$, S deviates from the true value like $S=S_{\rm true}+\delta S$. Since ν_i for $i=1\sim N_\ell$ are large numerical factors for a large $\ell_{\max}$, the relative error

$$\sum_{i=1}^{N_\ell} Y_{\ell,m}(\theta_i,\varphi)^*\delta S\nu_i \Big/ \sum_{i=1}^{N_\ell} Y_{\ell,m}(\theta_i,\varphi)^*S_{\rm true}\nu_i, \qquad (1.6)$$

becomes ~ 1 even for a small error $\delta S/S_{\rm true}=O(|\nu_i|^{-1})$. In the case when we want to determine a nonspherical AH in which contributions of high ℓ modes are significant, we need to adopt a large $\ell_{\max}$. Thus, in such a case, the two-surface of the AH will not be determined accurately by their method. (But, see [8] in which a devisal is proposed.)

In this paper, we propose a different method from theirs for a special family of 3D hypersurfaces: We assume that the 3D spacelike hypersurface has the π-rotation symmetry around the z axis [i.e., $h(\varphi,\theta)=h(\varphi+\pi,\theta)$] as well as the reflection symmetry with respect to the equatorial plane. This assumption is appropriate for many problems which we are interested in for the present, such as coalescence of BNS's of equal mass, the collapse of a rotating ellipsoid, and so on. (Note, however, that this method cannot be applied to determine the AH of each BH in coalescing binary BH's.) When such symmetries exist, the boundary condition for $h(\theta,\varphi)$ at the z axis becomes $h_{,\theta}=0$. In the present method, we solve the 2D elliptic-type equation for the AH as the boundary value problem under such a boundary condition. As shown below, in this method, the AH is accurately determined even when the geometry in 3D hypersurfaces is given numerically.

The paper is organized as follows: In Sec. II, we first derive the basic equation to determine the AH on the conformally flat 3D hypersurface, and then show a numerical method to solve the equation. In Sec. III, we review the initial value problem in general relativity and show numerical methods to solve the Hamiltonian and momentum constraints. In particular, a formulation to solve the momentum constraint equation accurately is presented. In order to show that the present method is accurate and efficient enough, we apply it to a variety of 3D hypersurfaces, i.e., to both time-symmetric and asymmetric 3D hypersurfaces, and to those obtained by solving the constraint equations analytically as well as numerically: In Sec. IV, we apply the AH finder to time-symmetric 3D hypersurfaces of many BH's close each other in order to determine the AH encompassing these BHs. In Sec. V, we apply it to time-asymmetric 3D hypersurfaces which are calculated numerically. In all cases, we show that the AH finder works well. Section VI is devoted to summary. Throughout this paper, we use the units of $c=G=1$.

II. APPARENT HORIZON FINDER IN 3D NUMERICAL RELATIVITY

A. Basic equation for apparent horizon

The AH is defined as the marginally outermost trapped surface [3]; i.e., outgoing light rays cannot expand from the AH. Expansion of the outgoing null vector is expressed as

$$\hat{\rho}=\nabla_\mu l_\nu(g^{\mu\nu}+n^\mu n^\nu-s^\mu s^\nu), \qquad (2.1)$$

where ∇_μ is the covariant derivative with respect to the spacetime metric $g_{\mu\nu}$, n^μ is the unit normal of a 3D spacelike hypersurface, s^μ is the unit normal of a two-surface of the AH, and l^μ is the outgoing null defined as $(n^\mu+s^\mu)/\sqrt{2}$. If a closed two-surface on which $\hat{\rho}$ vanishes everywhere exists, the AH exists. Before writing down the explicit equation of $\hat{\rho}=0$, we introduce the 3D metric and the extrinsic curvature which are defined, respectively, as

$$\gamma_{\mu\nu}=g_{\mu\nu}+n_\mu n_\nu, \qquad (2.2)$$

$$K_{ij}=-\gamma_i{}^\mu\gamma_j{}^\nu\nabla_\mu n_\nu. \qquad (2.3)$$

Then, from Eq. (2.1), the condition $\hat{\rho}=0$ is written as

$$K-K_{ij}s^is^j-D_is^i=0, \qquad (2.4)$$

where D_i is the covariant derivative with respect to γ_{ij} and K is the trace part of K_{ij}.

Denoting the location of the AH as $r=h(\theta,\varphi)$, s^i is expressed as

$$s_i=C\psi^2(1,-h_{,\theta},-h_{,\varphi}), \qquad (2.5)$$

where C is a normalization factor determined from $s^is_i=1$. In this paper, we only consider the conformal flat 3D metric, i.e., $\gamma_{ij}=\psi^4\delta_{ij}$ for simplicity. In this case, C becomes $(1+h_{,\theta}^2/h^2+h_{,\varphi}^2/h^2\sin^2\theta)^{-1/2}$. Substituting Eq. (2.5) into Eq. (2.4), the following equation is derived:

$$h_{,\theta\theta}+\cot\theta h_{,\theta}+\frac{h_{,\varphi\varphi}}{\sin^2\theta}-(2-\eta)h=\eta h+\frac{\psi^2h^2}{C^3}(K_{ij}s^is^j-K)+\frac{4}{\psi}\left(\psi_{,r}-\psi_{,\theta}\frac{h_{,\theta}}{h^2}-\psi_{,\varphi}\frac{h_{,\varphi}}{h^2\sin^2\theta}\right)\left(h^2+h_{,\theta}^2+\frac{h_{,\varphi}^2}{\sin^2\theta}\right)$$
$$+\frac{3}{h}\left(h_{,\theta}^2+\frac{h_{,\varphi}^2}{\sin^2\theta}\right)+\frac{1}{h^2\sin^2\theta}(2h_{,\theta}h_{,\varphi}h_{,\theta\varphi}-\cot\theta h_{,\varphi}^2h_{,\theta})-\frac{h_{,\theta}^2}{h^2\sin^2\theta}(\sin\theta\cos\theta h_{,\theta}+h_{,\varphi\varphi})$$
$$-\frac{h_{,\varphi}^2}{h^2\sin^2\theta}(h_{,\theta\theta}+\cot\theta h_{,\theta}),\tag{2.6}$$

where η is a constant and its value can be appropriately chosen to accelerate the convergence in numerical computation.

Since Eq. (2.6) is a 2D elliptic-type equation, it should be solved under appropriate boundary conditions at $\theta=\theta_{\max}$, $\theta_{\min}$, and $\varphi=\varphi_{\max}$, $\varphi_{\min}$. In this paper, we assume that the 3D hypersurface has the π-rotation symmetry around the z axis [$h(\varphi,\theta)=h(\varphi+\pi,\theta)$] as well as the reflection symmetry with respect to the equatorial plane. In this case, we must impose the boundary condition at $\varphi=0$ and π as $h(0,\theta)=h(\pi,\theta)$. Also, we need to impose the boundary conditions at $\theta=0$ and $\pi/2$. For the boundary condition at $\theta=\pi/2$, we simply impose $h_{,\theta}=0$ due to the reflection symmetry with respect to the equatorial plane. On the other hand, the boundary condition at $\theta=0$ is imposed as follows: Since the surface of the AH is smooth as well as the 3D hypersurface has the symmetries with respect to the π rotation around the z axis and the equatorial plane, the location of the AH can be expressed as

$$h(\theta,\varphi)=\sum_{\ell,m}a_{\ell,2m}Y_{\ell,2m}.\tag{2.7}$$

Notice that $Y_{\ell,m}$ is proportional to $\exp(im\varphi)P_{\ell,m}$, where $P_{\ell,m}$ is the associated Legendre polynomial, and $P_{\ell,m}$ behaves at $\theta\to0$ as

$$P_{\ell,m}\to\theta^m.\tag{2.8}$$

This means that $h(\theta,\varphi)$ behaves near $\theta=0$ as

$$h(\theta,\varphi)\to\text{const}+O(\theta^2).\tag{2.9}$$

Thus, we may also impose at $\theta=0$ as $h_{,\theta}=0$. We use these boundary conditions in numerical calculation.

Finally, we show the equation to calculate the area of the AH, $A_{\rm AH}$. The 2D geometry on the AH can be written as

$$dl^2=\psi^4\{(h_{,\theta}d\theta+h_{,\varphi}d\varphi)^2+h^2d\theta^2+h^2\sin^2\theta d\varphi^2\},$$
$$=\psi^4\{(h_{,\theta}^2+h^2)d\theta^2+2h_{,\theta}h_{,\varphi}d\theta d\varphi$$
$$+(h_{,\varphi}^2+h^2\sin^2\theta)d\varphi^2\},\tag{2.10}$$

and the determinant of the 2D metric becomes

$$\psi^8h^2(h^2\sin^2\theta+h_{,\theta}^2\sin^2\theta+h_{,\varphi}^2).\tag{2.11}$$

Hence, $A_{\rm AH}$ becomes

$$A_{\rm AH}=4\int_0^\pi d\varphi\int_0^{\pi/2}d\theta\psi^4h\sqrt{h^2\sin^2\theta+h_{,\theta}^2\sin^2\theta+h_{,\varphi}^2}.\tag{2.12}$$

B. Numerical method

The strategy to solve Eq. (2.6) is as follows: (1) We substitute a trial function $h^{(0)}(\theta,\varphi)$ into the right-hand side (RHS) of Eq.(2.6); (2) we solve an elliptic-type equation

$$h_{,\theta\theta}+\cot\theta h_{,\theta}+\frac{h_{,\varphi\varphi}}{\sin^2\theta}-(2-\eta)h=S(h^{(0)}),\tag{2.13}$$

as the boundary value problem; (3) we substitute a new $h(\theta,\varphi)$ obtained at (2) into the RHS of Eq. (2.6) and repeat this procedure until a sufficient convergence is achieved.

In solving Eq. (2.13), we first change the left-hand side (LHS) to a finite-difference form using

$$h_{,\theta\theta}=\frac{h_{i,j+1}-2h_{i,j}+h_{i,j-1}}{\delta\theta^2},\quad h_{,\theta}=\frac{h_{i,j+1}-h_{i,j-1}}{2\delta\theta},$$
$$h_{,\varphi\varphi}=\frac{h_{i+1,j}-2h_{i,j}+h_{i-1,j}}{\delta\varphi^2},\tag{2.14}$$

where i and j denote the grid point of φ and θ, respectively. We take the grid points as

$$\varphi_i=\left(i-\frac{1}{2}\right)\delta\varphi,\quad i=1\sim N_\varphi,$$
$$\theta_j=\left(j-\frac{1}{2}\right)\delta\theta,\quad j=1\sim N_\theta,\tag{2.15}$$

where N_φ and N_θ are grid numbers between $0<\varphi<\pi$ and $0<\theta<\pi/2$, respectively, and

$$\delta\varphi=\frac{\pi}{N_\varphi},\quad \delta\theta=\frac{\pi}{2N_\theta}.\tag{2.16}$$

At $i=1$ and N_φ, the finite differences for $h_{,\varphi\varphi}$ become

$$h_{,\varphi\varphi}=\frac{h_{2,j}-2h_{1,j}+h_{N_\varphi,j}}{\delta\varphi^2},\quad h_{,\varphi\varphi}=\frac{h_{1,j}-2h_{N_\varphi,j}+h_{N_\varphi-1,j}}{\delta\varphi^2}.\tag{2.17}$$

Also, at $j=1$ and N_θ, $h_{,\theta}$ and $h_{,\theta\theta}$ become

$$h_{,\theta\theta}=\frac{h_{i,2}-h_{i,1}}{\delta\theta^2},\quad h_{,\theta}=\frac{h_{i,2}-h_{i,1}}{2\delta\theta},$$

$$h_{,\theta\theta}=\frac{-h_{i,N_\theta}+h_{i,N_\theta-1}}{\delta\theta^2},\quad h_{,\theta}=\frac{h_{i,N_\theta}-h_{i,N_\theta-1}}{2\delta\theta}. \tag{2.18}$$

Then, the LHS of Eq. (2.6) is rewritten to the matrix equation as

$$M_{ij}h_j=S_i. \tag{2.19}$$

The schematic form of M_{ij} becomes

$$M_{ij}=\begin{pmatrix}
* & * & & & * & * & & & & & & & & & \\
* & * & * & & & & * & & & & & & & & \\
 & * & * & * & & & & * & & & & & & & \\
 & & * & * & * & & & & * & & & & & & \\
* & & & * & * & & & & & * & & & & & \\
* & & & & & * & * & & & * & * & & & & \\
 & * & & & & * & * & * & & & & * & & & \\
 & & * & & & & * & * & * & & & & * & & \\
 & & & * & & & & * & * & * & & & & * & \\
 & & & & * & * & & & * & * & & & & & * \\
 & & & & & * & & & & & * & * & & & * \\
 & & & & & & * & & & & * & * & * & & \\
 & & & & & & & * & & & & * & * & * & \\
 & & & & & & & & * & & & & * & * & * \\
 & & & & & & & & & * & * & & & * & *
\end{pmatrix}, \tag{2.20}$$

where * denotes a nonzero component, and if * is absent, the matrix components are equal to zero. (Note that the above form corresponds to the case $N_\varphi=5$ and $N_\theta=3$.) M_{ij} is not a symmetric matrix, but essentially has only five diagonal components. Thus, to solve this matrix equation, we make use of the ILUCGS (incomplete lower-upper decomposition and conjugate gradient squared) method [9] which is efficient when solving matrix equation in such a situation. In the ILUCGS method, we first carry out the ILU decomposition as $M_{ij}=L_{ik}D_{kk}U_{kj}-R_{ij}$, where

$$D_{ij}=\begin{cases} d_i & \text{for } j=i, \\ 0 & \text{otherwise,} \end{cases} \tag{2.21}$$

$$L_{ij}=\begin{cases} d_i^{-1} & \text{for } j=i, \\ M_{ij} & \text{for } j=i-1,\ i-N_\varphi, \\ 0 & \text{otherwise,} \end{cases} \tag{2.22}$$

$$U_{ij}=\begin{cases} d_i^{-1} & \text{for } j=i, \\ M_{ij} & \text{for } j=i+1,\ i+N_\varphi, \\ 0 & \text{otherwise,} \end{cases} \tag{2.23}$$

and d_i is determined from the condition

$$L_{ik}D_{kk}U_{ki}=M_{ii}. \tag{2.24}$$

R_{ij} has two diagonal components as

$$R_{ij}\begin{cases} \neq 0 & \text{for } j=i\pm N_\varphi\mp 1, \\ =0 & \text{otherwise,} \end{cases} \tag{2.25}$$

and calculated from $L_{ik}D_{kk}U_{kj}-M_{ij}$. Hence, $(i,i\pm N_\varphi\mp 1)$ components in M_{ij} are absorbed in R_{ij}. Note that the acceleration parameter η [see Eq. (2.6)] is chosen as ~ 1 in making M_{ij}. Once the ILU decomposition is completed, we rewrite Eq. (2.19) as

$$[\mathbf{I}-\mathbf{U}^{-1}\mathbf{D}^{-1}\mathbf{L}^{-1}\mathbf{R}]\mathbf{h}=\mathbf{U}^{-1}\mathbf{D}^{-1}\mathbf{L}^{-1}\mathbf{S}, \tag{2.26}$$

where $\mathbf{I}$ is the unit matrix. Then, Eq. (2.26) is solved by the CGS method. In the Appendix, we also show the numerical scheme in the case where the 3D hypersurface has symmetries with respect to x-y, y-z, and z-x planes.

It should be also noticed that we use a relaxation technique in substituting $h(\theta,\varphi)$ into the RHS of Eq. (2.26) [i.e., in procedure (2)]. We determine the trial value as

$$h_{\rm trial}^{(n+1)}=h^{(n)}\xi+h_{\rm trial}^{(n)}(1-\xi), \tag{2.27}$$

where $h^{(n)}$ is a solution of Eq. (2.13) for $S(h_{\rm trial}^{(n)})$. ξ is an acceleration parameter and chosen as ~ 0.5.

Finally, we emphasize the following point: The solution of Eq. (2.13) in each step of iteration is guaranteed to be regular because the matrix operator on the LHS of Eq. (2.13) is taken so as for **h** to become regular. As a result, when we substitute a new trial function calculated from Eq. (2.27) into the RHS of Eq. (2.13), the RHS of Eq. (2.13) is also guaranteed to be regular. Hence, if we give an initial trial function $h^{(0)}$ which is a regular function anywhere, the final solution of $h(\theta,\varphi)$ is also guaranteed to be regular. This is the essential reason why the present method works well.

III. INITIAL VALUE PROBLEMS

In order to test the method described in Sec. II, we must prepare 3D spacelike hypersurfaces. In general relativity, the Hamiltonian and momentum constraints must be satisfied in each 3D hypersurface. This means that to prepare a 3D hypersurface, we need to solve these constraint equations. In the case where the 3D hypersurface is assumed to be conformally flat and $K=0$, they are, respectively, written as [10]

$$\Delta\psi=-2\pi\rho_h\psi^5-\frac{1}{8\psi^7}A_{ij}A^{ij}\equiv-4\pi S_\psi, \tag{3.1}$$

and

$$\widetilde{D}_i A^i_j=8\pi\psi^6 J_j, \tag{3.2}$$

where $\widetilde{D}_i$ is the covariant derivative with respect to δ_{ij} and Δ is the Laplacian of flat space. In the following, we use the Cartesian coordinate, so that $\widetilde{D}_i=\partial_i$. A_{ij} is defined as ψ^2K_{ij}, and its indices are raised and lowered by δ_{ij}, i.e., $A_{ij}=A^{ij}=A_i{}^j$. ρ_h and J_i are defined from the energy-momentum tensor as

$$\rho_h=T_{\mu\nu}n^\mu n^\nu,\quad J_i=-T_{\mu\nu}n^\mu\gamma^\nu_i. \tag{3.3}$$

If we assume the absence of the transverse-traceless part of A_{ij}, we can rewrite A_{ij} as [10]

$$A_{ij}=W_{i,j}+W_{j,i}-\tfrac{2}{3}\delta_{ij}W_{k,k}. \tag{3.4}$$

Then, Eq. (3.2) becomes

$$\Delta W_i+\tfrac{1}{3}W_{k,ki}=8\pi\psi^6J_i. \tag{3.5}$$

This is the coupled elliptic-type equation for W_x, W_y, and W_z, and it is not a desired form in numerical calculation. To decompose the coupling of each component of W_i, previous authors [11,12] have introduced methods of decomposition of this equation. However, in their methods, the Poisson equations with noncompact source appear as a result of the decomposition. In 3D numerical relativity, the grid number we can adopt is restricted, and it seems difficult to improve accuracy in solving such an equation in the restricted grid number. Thus, we rewrite W_i as

$$W_i=B_i-\frac{1}{8}\{\chi_{,i}+(B_kx^k)_{,i}\}, \tag{3.6}$$

where B_i and χ are vector and scalar potentials, and $x^k=(x,y,z)$. Then, the LHS of Eq. (3.5) becomes

$$\Delta B_i-\tfrac{1}{6}(\Delta\chi+\Delta B_kx^k)_{,i}. \tag{3.7}$$

Hence, Eq. (3.5) may be decomposed into the two equations

$$\Delta B_i=8\pi\psi^6J_i\equiv8\pi S_i, \tag{3.8}$$

$$\Delta\chi=-8\pi\psi^6J_ix^i\equiv-8\pi S_ix^i. \tag{3.9}$$

Thus, the source terms of Poisson equations for B_i and χ are compact as long as compact matter is concerned. We emphasize again that this decomposition of W_i is very useful to obtain W_i accurately.

In the following, we will take $S_i=J_i\psi^6$ as (1) $S_i=0$ (i.e., $K_{ij}=0$), or (2) $S_i=S(\mathbf{x})a_{ij}x^j$, where a_{ij} is a matrix and chosen as

$$a_{ij}=\begin{pmatrix}\kappa+\sigma & -\omega & 0\\ \omega & \kappa-\sigma & 0\\ 0 & 0 & 0\end{pmatrix}. \tag{3.10}$$

Hence, we do not solve B_z in the following. In case (1), we only need to solve the Poisson equation for ψ, and in case (2), we first calculate the Poisson equations for B_i and χ to give A_{ij}, and then Eq. (3.1) is solved.

When we solve the Poisson equations shown above numerically, we adopt homogeneous or inhomogeneous Cartesian grids which cover $-L\leqslant x$, $y\leqslant L$, and $0\leqslant z\leqslant L$, where L is a constant, in order to set up a finite-differencing equation. Inhomogeneous grids are taken as

$$\delta x_i=\alpha\delta x_{i-1},\quad \delta y_j=\alpha\delta y_{j-1},\quad \delta z_k=\alpha\delta z_{k-1}, \tag{3.11}$$

where $\delta x_i=x_{i+1}-x_i$, $\delta y_j=y_{j+1}-y_j$, $\delta z_k=z_{k+1}-z_k$ and α is chosen as $1<\alpha\leqslant1.05$. At the outer boundary ($|x|$, $|y|$, and $z=L$), we impose boundary conditions as

$$\psi=1+\frac{M}{2r}+O(r^{-3}), \tag{3.12}$$

$$B_i=-\frac{2n^x}{r^2}\int S_ixdV-\frac{2n^y}{r^2}\int S_iydV+O(r^{-4}), \tag{3.13}$$

$$\chi=\frac{2}{r}\int S_ix^idV+O(r^{-3}), \tag{3.14}$$

where $n^i=x^i/r$ and M is the gravitational mass of the system calculated by

$$M=2\int S_\psi dV. \tag{3.15}$$

Thus, the Poisson equations for ψ and χ are solved by the same Poisson solver, but that for B_i is different from it. Hence, we need two types of the Poisson solvers. In both cases, we impose the reflection symmetry condition with respect to the equatorial plane $z=0$.

The finite-differencing equation for these Poisson equations becomes

$$C_{ij}X_j=Y_i, \tag{3.16}$$

where $C_{ij}=C_{ji}$ has seven diagonal components, and X_i and Y_i are vectors. To solve this type of matrix equation, we use the ICCG (incomplete Choleskii and conjugate gradients) method [9], which is a similar method to the ILUCGS method: In this method, the matrix $\mathbf{C}$ is decomposed into $\mathbf{LDL}^T-\mathbf{R}$, where $L^T_{ij}=L_{ji}$, because of symmetry of $\mathbf{C}$. Then, we transform Eq. (3.16) into the following matrix equation:

$$[\mathbf{I}-(\mathbf{LDL}^T)^{-1}\mathbf{R}]\mathbf{X}=(\mathbf{LDL}^T)^{-1}\mathbf{Y}, \tag{3.17}$$

and solve Eq. (3.17) by the CG method.

Accuracy of the Poisson solvers are checked by comparing numerical solutions with the exact solutions. For example, if we choose the density as

$$\rho=\begin{cases}\rho_0(1-r_+^2/r_0^2) & \text{for } r_+<r_0,\\ \pm\rho_0(1-r_-^2/r_0^2) & \text{for } r_-<r_0,\\ 0 & \text{otherwise,}\end{cases} \tag{3.18}$$

where ρ_0 is a constant, $r_\pm=\sqrt{(x\mp x_c)^2+(y\mp y_c)^2+z^2}$ and x_c, y_c, r_0 are constants $<L/2$, then the following ϕ is the solution of the Poisson equation $\Delta\phi=4\pi\rho$:

$$\phi=\begin{cases}-M_0/r_+\mp M_0/r_- & \text{for } r_+, r_-\geqslant r_0,\\ -M_0/r_+\pm\pi\rho_0 f(r_-) & \text{for } r_+\geqslant r_0, r_-<r_0,\\ \pi\rho_0 f(r_+)\mp M_0/r_- & \text{for } r_-\geqslant r_0, r_+<r_0,\\ \pi\rho_0 f(r_+)\pm\pi\rho_0 f(r_-) & \text{for } r_+, r_-<r_0,\end{cases} \tag{3.19}$$

where $M_0=8\pi\rho_0 r_0^3/15$, and

$$f(r)=\frac{2}{3}r^2-\frac{1}{5r_0^2}r^4-r_0^2. \tag{3.20}$$

The solution of the upper sign can be used to check whether the scalar-type Poisson solver works well or not, and the other one is for the vector-type Poisson solver. We compared the numerical solutions with the exact ones for several combinations of (x_c, y_c, r_0).

In Fig. 1, we show the absolute value of the relative error, $|1-(\text{numerical solutions})/(\text{exact solutions})|$, in the equatorial plane $(0\leqslant x,y\leqslant L)$ for the Poisson solvers of the scalar-type potential [Fig. 1(a)] as well as the vector-type potential [Fig. 1(b)] in the case where $x_c=r_0=L/3$ and $y_c=0$ as an example. In this case, we use the homogeneous grid with a grid number of (97,97,49). For the scalar-type Poisson solver, the relative error is always less than $\sim 10^{-3}$ within $r\sim 2L/3$ although around the outer boundary it often becomes as large as $\sim 10^{-2}$. For the vector-type Poisson solver, it is also less than $\sim 2\times 10^{-3}$ within $r\sim 2L/3$ although it becomes $\sim 2\times 10^{-2}$ at the outer boundary. Thus, the accuracy of A_{ij} near the outer boundary is not so good. However, $A_{ij}A^{ij}$ around the outer boundary is not large compared with that in the inner region because A_{ij} behaves as $\to r^{-3}$ for $r\to\infty$. Hence, the error itself does not contribute to the source term of ψ so much.[1] Also, we will find the AH far from the outer boundary (see Sec. V), so that the accuracy of the Poisson solvers seems sufficient.

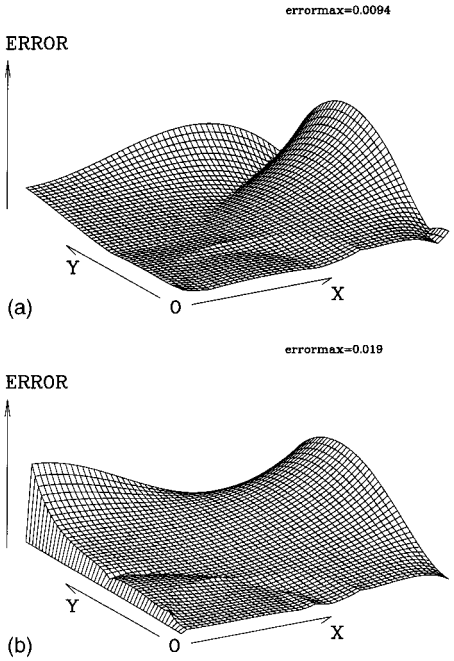

FIG. 1. Accuracy of the Poisson solvers for the scalar-type (a) and vector-type potentials (b). In each figure, the relative error in the equatorial plane $(0\leqslant x,y\leqslant L)$ is shown.

IV. APPARENT HORIZON ENCOMPASSING MANY BLACK HOLES

In this section, we apply the AH finder to time-symmetric 3D spacelike hypersurfaces of many BH's. If these BH's are close enough, the AH, which encompasses them, will exist. The purpose of this section is to determine it.

A geometry which represents N-BH's of each mass m_i at an arbitrary spatial point $\mathbf{r}_i$ at a moment of time symmetry (i.e., $A_{ij}=0$) may be conformally flat, and the conformal factor can be written as [13,14,15]

$$\psi=1+\sum_{i=1}^{N}\frac{m_i}{2|\mathbf{r}-\mathbf{r}_i|}. \tag{4.1}$$

In this paper, we set $m_i=2\mu/N$ (i.e., $M=2\mu$) and take $\mathbf{r}_i=(x_i, y_i, z_i)$ as

$$x_i=\frac{r_{\rm BH}}{2}\cos\left(\frac{2\pi}{N}i+\varphi_c\right),\quad y_i=\frac{r_{\rm BH}}{2}\sin\left(\frac{2\pi}{N}i+\varphi_c\right),\quad z_i=0, \tag{4.2}$$

where $r_{\rm BH}$ and φ_c are constants.

In the case $N=2$, the 3D hypersurface is axisymmetric around the axis connecting two centers of BH's. If the axis is chosen as the z axis, Eq. (2.6) becomes the following ordinary differential equation:

[1]But, as mentioned in Sec. V, $A_{ij}A^{ij}$ does contribute even at $r\sim L$ unless L is large enough.

$$h_{,\theta\theta}+\cot\theta h_{,\theta}-(2-\eta)h$$
$$=\eta h+\psi^2 h^{-1}(h^2+h_{,\theta}^2)^{3/2}(K_{ij}s^i s^j-K)$$
$$+\frac{4}{\psi}\left(\psi_{,r}-\psi_{,\theta}\frac{h_{,\theta}}{h^2}\right)(h^2+h_{,\theta}^2)+\frac{3}{h}h_{,\theta}^2-\frac{h_{,\theta}^3\cot\theta}{h^2}. \quad (4.3)$$

This equation is solved under the boundary conditions $h_{,\theta}=0$ at $\theta=0$ and $\pi/2$. In the axisymmetric case, the AH is easily determined with a desired accuracy as has been investigated so far [15,16,17,18]. So that, first of all, we apply the 3D AH finder to determine the AH encompassing two-BH's which are not located in the z axis, but in the equatorial plane (i.e., located in the non-axisymmetric configurations around the z axis), and compare the result with the axisymmetric one calculated by the 2D AH finder. [Hereafter, we call the numerical code to solve Eq. (4.3) ''the 2D AH finder.'' On the other hand, we call the numerical code to solve Eq. (2.6) ''the 3D AH finder.'']

For the two-BH case, Cadez showed that there exists the AH which encompasses two BH's when $r_{\rm BH}$ is less than $\sim 1.53\mu$ [16]. Hence, we investigate the AH changing $r_{\rm BH}$ from 0 to 1.53μ as well as changing grid numbers, N_φ and N_θ. We also change φ_c from 0 to $\pi/2$, but the results, of course, do not depend on φ_c. An initial trial function $h^{(0)}$ is chosen as $h_0-h_1\cos\theta$, where $0.9\leqslant h_0/\mu\leqslant 1.1$ and $0\leqslant h_1/\mu\leqslant 0.5$ are constants. For $r_{\rm BH}\leqslant 1.5\mu$, the AH is determined with a sufficient accuracy within 10 iterations, although about ~ 100 iterations are needed for $r_{\rm BH}\sim 1.53\mu$. In Table I, we show the area of the AH as a function of $r_{\rm BH}$. The area is shown in units of $64\pi\mu^2$. The second column shows the results by means of the 2D AH finder, and third to seventh columns show results by means of the 3D AH finder with $N_\varphi=N_\theta=16$, 32, 48, 64, and 100, respectively. Note that for the case $r_{\rm BH}=1.53\mu$ with $N_\varphi=N_\theta=16$, the AH cannot be found. This is simply because the coarse grid fails to resolve the highly distorted surface of the AH.

In Fig. 2, we show numerical errors of the area of AH as a function of $N_\varphi(=N_\theta)$ for the cases $r_{\rm BH}/\mu=1.4$ (solid circles) and 1.52 (open circles). The numerical error is defined as

TABLE I. Area of the AH encompassing two-BH's at a moment of time symmetry as a function of $r_{\rm BH}$. The area is shown in units of $16\pi M^2$, where M is the gravitational mass of the system. The first column denotes $r_{\rm BH}$ in units of $\mu=M/2$. The second column shows results calculated by the 2D AH finder, and the third to seventh columns show results by the 3D AH finder with different grid numbers (N_φ,N_θ). ''×'' means that the AH finder fails to find the AH.

$r_{\rm BH}$	2D cal.	(16,16)	(32,32)	(48,48)	(64,64)	(100,100)
1.53	0.97710	×	0.97540	0.97637	0.97670	0.97693
1.52	0.97801	0.97194	0.97659	0.97738	0.97766	0.97786
1.50	0.97960	0.97466	0.97840	0.97906	0.97930	0.97947
1.40	0.98550	0.98260	0.98478	0.98518	0.98532	0.98543
1.20	0.99260	0.99141	0.99230	0.99247	0.99253	0.99257
1.00	0.99650	0.99613	0.99641	0.99646	0.99648	0.99649

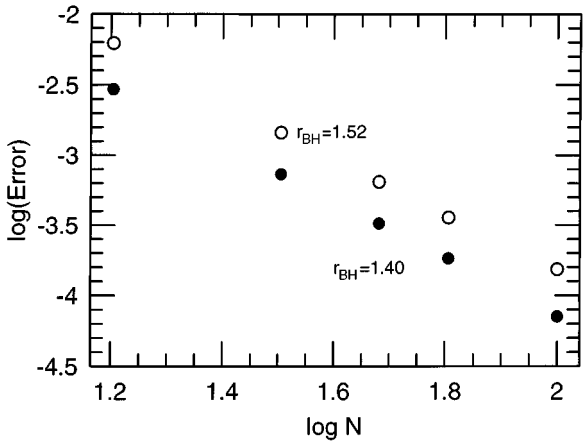

FIG. 2. Numerical errors of the area of AH [Eq. (4.4)] as a function of $N_\varphi(=N_\theta)$ for the cases $r_{\rm BH}/\mu=1.4$ (solid circles) and 1.52 (open circles). The logarithm is to base 10.

$$1-\frac{\text{area of the AH determined by 3D AH finder}}{\text{area of the AH determined by 2D AH finder}}. \quad (4.4)$$

The figure shows that the numerical algorithm is indeed second-order convergent.

In Fig. 3, we compare the location of the AH determined

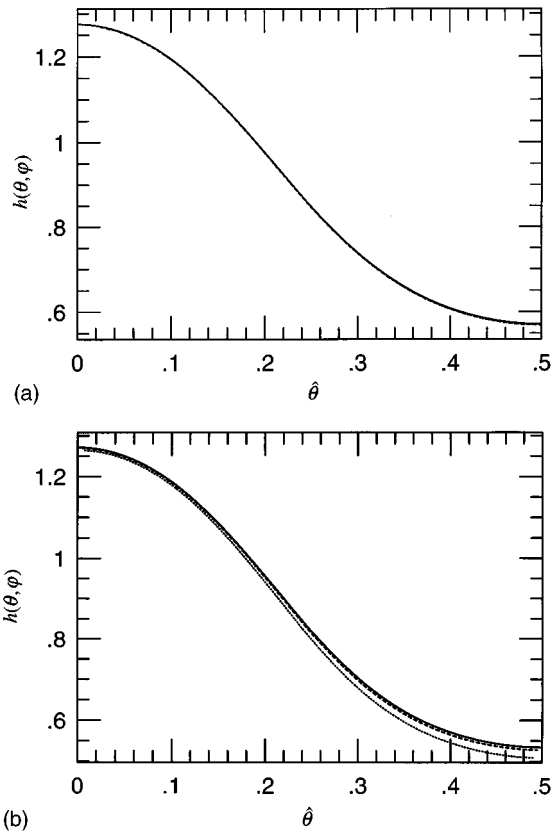

FIG. 3. Location of the AH encompassing two-BH's for the case $r_{\rm BH}/\mu=1.52$ (a) and 1.53 (b). The horizontal axis shows $\hat{\theta}$ (see text) and the vertical axis shows the radius of the AH. Solid, dotted, and dashed lines denote the results by the 2D AH finder, 3D AH finder of (32,32) grids, and 3D AH finder of (48,48) grids, respectively.

by the 3D AH finder with that by the 2D AH finder for the case $r_{\rm BH}=1.52\mu$ and 1.53μ. The horizontal axis denotes $\hat{\theta}=\theta/\pi$ for the 2D case and $\hat{\theta}=1/2-\theta/\pi$ for the 3D case ($\varphi=0$), and the vertical axis shows the radius of the AH in each $\hat{\theta}$. Solid, dotted, and dashed lines denote results by the 2D AH finder, the 3D AH finder of $N_\varphi=N_\theta=32$, and of $N_\varphi=N_\theta=48$, respectively. These results show that (1) when the AH is not so distorted, a grid number of $N_\varphi=N_\theta=32$ is enough and (2) the numerical scheme works fairly well even for the highly distorted AH if we take the grid number of $N_\varphi=N_\theta=48$. Hence, we adopt $N_\varphi=N_\theta=48$ as a grid number in the following. In this case, the numerical error of $A_{\rm AH}$ is expected to be less than 0.1% for any case. We note, however, that unless the AH is so distorted, we do not need such a large number of the grid to guarantee that the accuracy for $A_{\rm AH}$ is better than $\sim 0.1\%$.

Then, we present numerical results for the cases of many BH's. Before showing numerical results, we comment on the limit $N\to\infty$. In this case, Eq. (4.1) becomes

$$\psi=1+\lim_{N\to\infty}\frac{\mu}{N}\sum_{k=1}^{N}\frac{1}{\sqrt{r^2+r_{\rm BH}^2-2rr_{\rm BH}\sin\theta\cos(\varphi-2\pi k/N)}},$$

$$=1+\frac{\mu}{2\pi}\int_0^{2\pi}d\varphi'\frac{1}{\sqrt{r^2+r_{\rm BH}^2-2rr_{\rm BH}\sin\theta\cos\varphi'}},$$

$$=1+\frac{2\mu}{\pi\sqrt{r^2+r_{\rm BH}^2+2rr_{\rm BH}\sin\theta}}K(k), \tag{4.5}$$

where $K(k)$ is a complete elliptic integral of the first kind as

$$K(k)=\int_0^{\pi/2}\frac{d\phi}{\sqrt{1-k^2\sin^2\phi}}, \tag{4.6}$$

and

$$k^2=\frac{4rr_{\rm BH}\sin\theta}{r^2+r_{\rm BH}^2+2rr_{\rm BH}\sin\theta}. \tag{4.7}$$

This conformal factor agrees with that of ring whose ρ_h is

$$\rho_h\psi^5=\frac{\mu}{\pi r_{\rm BH}}\delta(r-r_{\rm BH})\delta\left(\theta-\frac{\pi}{2}\right). \tag{4.8}$$

This means that when N is large enough and also $r_{\rm BH}$ is not so large that the two-surface of the AH is nearly spherical, the AH encompassing the many BH's should be approximately the same as that for the ring. The AH for the ring is easily and accurately determined by the 2D AH finder. Hence, by comparing the AH for N-BH's determined by the 3D AH finder with the AH for the ring determined by the 2D AH finder, we can carry out the code check of the 3D AH finder, again.

In Table II, we show the area of the AH for 4, 6, 8, 12, 16, and 24 BH's and the ring as a function of $r_{\rm BH}$. In Fig. 4, we also show the area of the AH as a function of $r_{\rm BH}$. The solid line denotes numerical results for the ring determined by the 2D AH finder, and squares, hexagons, triangles, and circles denote those for BH's of $N=4$, 6, 8, and 16, respectively,

TABLE II. Area of the AH encompassing the ring and N-BH's at a moment of time symmetry as a function of $r_{\rm BH}$ in units of μ. The area is shown in units of $16\pi M^2$. The AH encompassing ring is determined by the 2D AH finder, while the AH encompassing N-BH's is determined by the 3D AH finder with $(N_\varphi,N_\theta)=(48,48)$ (so that, the numerical error will be less than 0.1%). ''No'' means that the AH encompassing N-BH's do not exist.

$r_{\rm BH}$	Ring	24BH's	16BH's	12BH's	8BH's	6BH's	4BH's
2.10	0.976	No	No	No	No	No	No
2.00	0.982	No	No	No	No	No	No
1.90	0.986	0.984	0.983	No	No	No	No
1.80	0.989	0.988	0.988	0.988	0.986	No	No
1.70	0.991	0.991	0.991	0.991	0.990	0.989	No
1.60	0.993	0.993	0.993	0.993	0.993	0.992	0.989
1.50	0.995	0.995	0.995	0.995	0.995	0.995	0.993
1.40	0.996	0.996	0.996	0.996	0.996	0.996	0.995
1.20	0.998	0.998	0.998	0.998	0.998	0.998	0.998
1.00	0.999	0.999	0.999	0.999	0.999	0.999	0.999

which are determined by the 3D AH finder. Note that, in all cases, the AH which encompasses N-BH's disappears when $r_{\rm BH}$ becomes larger than a critical separation $r_{\rm crit}$, where $r_{\rm crit}\sim 1.66-1.67\mu$ for $N=4$, $r_{\rm crit}\sim 1.76-1.77\mu$ for $N=6$, $r_{\rm crit}\sim 1.82-1.83\mu$ for $N=8$, $r_{\rm crit}\sim 1.89-1.90\mu$ for $N=12$, $r_{\rm crit}\sim 1.91-1.92\mu$ for $N=16$, $r_{\rm crit}\sim 1.92-1.93\mu$ for $N=24$, and $r_{\rm crit}\sim 2.13-2.14\mu$ for ring. From Fig. 4, we soon find that when $r_{\rm BH}$ is sufficiently smaller than $r_{\rm crit}$, the area of the AH for N-BH's is nearly equal to that for the ring. This fact also supports that our numerical scheme works well.

Finally, we comment on the shape of the two-surface of the AH. Irrespective of N, the two-surface of the AH becomes nonspherical near $r_{\rm crit}$. In Fig. 5, we plot bird's-eye-views of the two-surface of the AH for the case $r_{\rm BH}=1.2$, 1.5, and 1.66 of $N=4$ as an example. We can see that with increase of $r_{\rm BH}$, the nonspherical nature of the two-surface of the AH is remarkable.

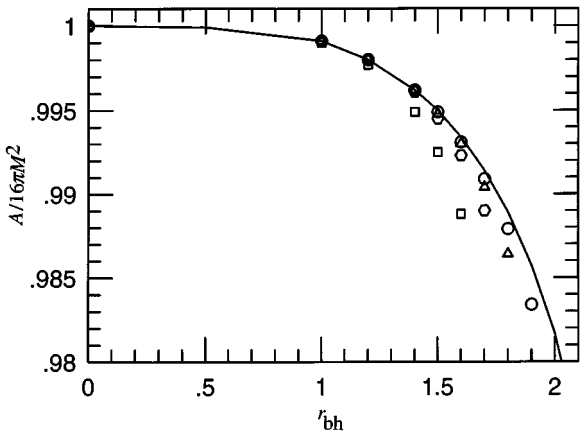

FIG. 4. The area of the AH which encompasses N-BH's, where $N=4$ (squares), 6 (hexagons), 8 (triangles), and 16 (circles), and ring (solid line), as a function of $r_{\rm BH}$. The area is shown in units of $16\pi M^2$.

V. APPARENT HORIZONS FOR TIME-ASYMMETRIC 3D HYPERSURFACES

In this section, we prepare time-asymmetric 3D hypersurfaces from Eqs. (3.1), (3.4), (3.6), (3,8), and (3.9), and apply the 3D AH finder to them. First, we consider the case when equations for B_i and χ can be analytically obtained as follows. The solution of a vector Poisson equation

$$\Delta P_i = 4\pi\rho(r)x^i, \tag{5.1}$$

where

$$\rho(r)=\begin{cases}\rho_0(1-r^2/r_0^2) & \text{for } r\leqslant r_0,\\ 0 & \text{for } r>r_0,\end{cases} \tag{5.2}$$

is written as

$$P_i=\begin{cases}4\pi\rho_0 x^i(-r_0^2/12+r^2/10-r^4/28r_0^2) & \text{for } r\leqslant r_0,\\ -8\pi\rho_0 r_0^5 x^i/105r^3 & \text{for } r>r_0.\end{cases} \tag{5.3}$$

Also, the solutions of the following scalar-type Poisson equations,

$$\Delta Q_1 = 4\pi\rho(r)(x^2-y^2), \tag{5.4}$$

$$\Delta Q_2 = 4\pi\rho(r)\left(z^2-\frac{r^2}{3}\right), \tag{5.5}$$

$$\Delta Q_3 = 4\pi\rho(r)r^2, \tag{5.6}$$

are, respectively, written as

$$Q_1=\begin{cases}4\pi\rho_0(-r_0^2/20+r^2/14-r^4/36r_0^2)(x^2-y^2) & \text{for } r\leqslant r_0,\\ -8\pi\rho_0 r_0^7(x^2-y^2)/315r^5 & \text{for } r>r_0,\end{cases} \tag{5.7}$$

$$Q_2=\begin{cases}4\pi\rho_0(-r_0^2/20+r^2/14-r^4/36r_0^2)(z^2-r^2/3) & \text{for } r\leqslant r_0,\\ -8\pi\rho_0 r_0^7(z^2-r^2/3)/315r^5 & \text{for } r>r_0,\end{cases} \tag{5.8}$$

$$Q_3=\begin{cases}4\pi\rho_0(-r_0^4/12+r^4/20-r^6/42r_0^2) & \text{for } r\leqslant r_0,\\ -8\pi\rho_0 r_0^5/35r & \text{for } r>r_0.\end{cases} \tag{5.9}$$

Hence, if we choose $S(\mathbf{x})=\rho(r)$, then the solutions of B_i and χ are simply written as

$$B_x = -2\omega P_y + 2(\kappa+\sigma)P_x, \tag{5.10}$$

$$B_y = 2\omega P_x + 2(\kappa-\sigma)P_y, \tag{5.11}$$

$$\chi = -2\sigma Q_1 + 2\kappa\left(Q_2-\frac{2}{3}Q_3\right). \tag{5.12}$$

Note that, in all cases, the linear momentum of the system vanishes, while the angular momentum J_φ of the system is written as

$$J_\varphi = \frac{8\pi}{105}\rho_0 r_0^5\omega = \frac{1}{7}M_0 r_0^2\omega. \tag{5.13}$$

We also give a very simple expression for ρ_h as

$$\rho_h\psi^5 = \rho(r). \tag{5.14}$$

Thus, in the time-symmetric case, $\kappa=\sigma=\omega=0$, ψ becomes

$$\psi\equiv\psi_0=\begin{cases}1-\pi\rho_0 f(r)/2 & \text{for } r\leqslant r_0,\\ 1+M_0/2r & \text{for } r>r_0,\end{cases} \tag{5.15}$$

where the gravitational mass of the system (M) is equal to M_0. In the following, we will set $M_0=2$ and $r_0=0.9$. In the time-symmetric case, the AH exists at $h(\theta,\varphi)=1$ because the 3D hypersurface is spherical symmetric and $M>2r_0$. However, this is not the case when one of three parameters, (κ,σ,ω), is not zero.

We consider six cases: (a) $\kappa\neq 0$ and $\sigma=\omega=0$, (b) $\sigma\neq 0$ and $\kappa=\omega=0$, (c) $\omega\neq 0$ and $\kappa=\sigma=0$, (d) $\kappa=\sigma\neq 0$ and $\omega=0$, (e) $\sigma=\omega\neq 0$ and $\kappa=0$, (f) $\kappa=\sigma=\omega\neq 0$. For cases (a), (c), and (d), the 3D hypersurfaces are axisymmetric, while for other cases, they are nonaxisymmetric. Note that for case $\kappa=\pm\sigma\neq 0$ and $\omega=0$, the matter is purely collapsing or expanding in the x or y direction, and for case (c), the matter is purely rotating around the z axis.

In solving the Poisson equation for ψ, we adopt homogeneous as well as inhomogeneous grids with various grid spacings, but fixing grid number as $(N_x,N_y,N_z)=(109,109,55)$ in order to see the dependence of results on the choice of grids. We find that fluctuations of the gravitational mass and the area of the AH is less than 1% if the amplitude of A_{ij} is small (i.e., $|\kappa|$, $|\sigma|$, $|\omega|\sim 1-2$), but they become larger than 1% when $|\kappa|$, $|\sigma|$, $|\omega|$ are larger than ~ 5. The fluctuations mainly come from the volume integral of $A_{ij}A^{ij}\psi^{-7}$ in Eq. (3.15) which is evaluated in estimation of M and thus used when imposing the outer boundary condition. It is not easy to suppress this

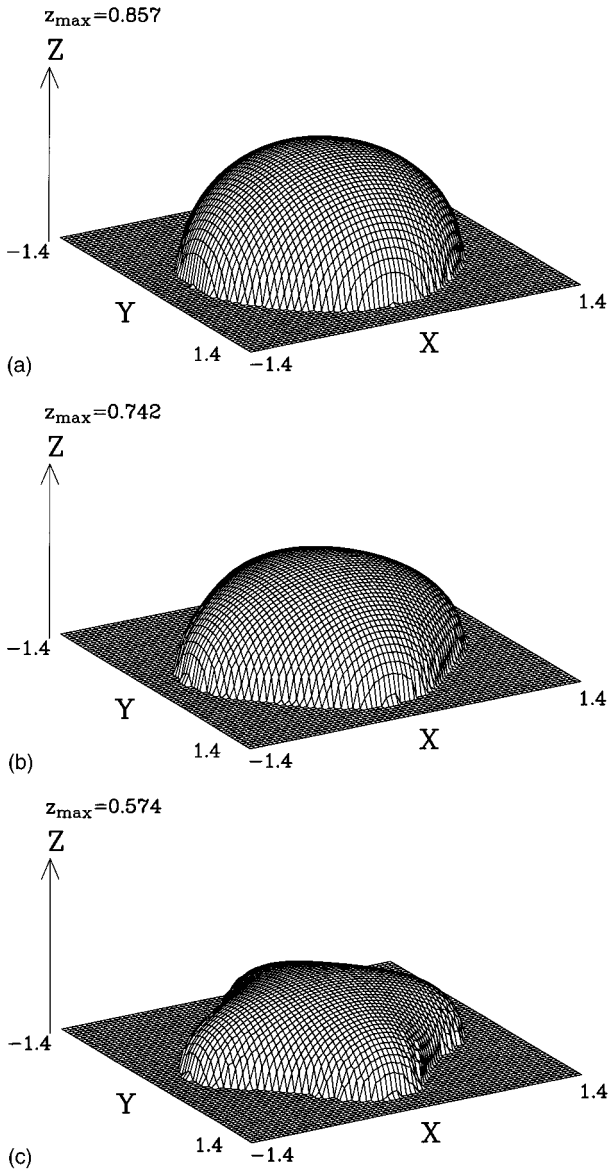

FIG. 5. Bird's-eye views of the AH for the case $r_{BH}/\mu=1.2$ (a), 1.5 (b), and 1.66 (c) of $N=4$.

numerical error due to the following reasons: (I) when we use a coarse grid spacing, the truncation error becomes very large because $A_{ij}A^{ij}$ changes rapidly around $r\sim 1$, and a coarse grid cannot resolve it correctly; (II) we will underestimate M for the case where we take a small grid spacing and as a result, L is not sufficiently large, because $A_{ij}A^{ij}$ behaves as $\rightarrow r^{-6}$ at $r\rightarrow\infty$. To estimate how much the error of the gravitational mass is, it is appropriate to see the quantity

$$I(R)\equiv\int_{r\leq R}A_{ij}A^{ij}\psi_0^{-7}d^3x. \tag{5.16}$$

We found that $I(4)/I(\infty)\simeq 0.88$, $I(5)/I(\infty)\simeq 0.92$, and $I(6)/I(\infty)\simeq 0.95$ irrespective of cases (a)−(f). Thus, for case

TABLE III. Numerical results on time-asymmetric initial data and the apparent horizon on it for various combinations of (κ,σ,ω). The third to fifth columns show the gravitational mass of system(M), $(h_x,h_y,h_z)=[h(0,\pi/2),\ h(\pi/2,\pi/2),\ h(0,0)]$, and the area of the AH in units of $16\pi M^2$. The Poisson equation for the conformal factor is calculated using the homogeneous grid with $(N_x,N_y,N_z)=(109,109,55)$ and $\delta x=\delta y=\delta z=0.09$. For the case $M\sim 2.00$, the numerical error of M, (h_x,h_y,h_z) and A_{AH} is less than 1%, but for $M>2.1$, the error is $1-2$ %.

Cases	(κ,σ,ω)	M	(h_x,h_y,h_z)	$A_{AH}/16\pi M^2$
(a)	(0,0,0)	2.00	(1.00,1.00,1.00)	1.00
	(1,0,0)	2.00	(0.92,0.92,0.93)	1.00
	(−1,0,0)	2.00	(1.08,1.08,1.06)	1.00
	(−2,0,0)	2.02	(1.16,1.16,1.13)	1.01
	(−5,0,0)	2.11	(1.40,1.40,1.33)	1.02
(b)	(0,2,0)	2.01	(0.97,1.02,1.00)	1.00
	(0,5,0)	2.07	(0.94,1.04,0.99)	0.98
	(0,8,0)	2.17	(0.90,1.05,0.97)	0.95
(c)	(0,0,±2)	2.02	(1.00,1.00,1.00)	0.99
	(0,0,±5)	2.16	(0.98,0.98,0.98)	0.95
	(0,0,±8)	2.35	(0.94,0.94,0.94)	0.90
(d)	(1,1,0)	2.01	(0.91,0.93,0.93)	1.00
	(−1,−1,0)	2.01	(1.08,1.06,1.06)	1.00
	(−2,−2,0)	2.03	(1.18,1.13,1.13)	1.00
	(−5,−5,0)	2.17	(1.46,1.33,1.33)	1.00
(e)	(0,1,1)	2.01	(0.99,1.01,1.00)	1.00
	(0,2,2)	2.04	(0.97,1.02,0.99)	0.99
	(0,5,5)	2.22	(0.92,1.01,0.97)	0.94
	(0,8,8)	2.46	(0.84,0.95,0.90)	0.88
(f)	(1,1,1)	2.01	(0.91,0.93,0.93)	1.00
	(−1,−1,−1)	2.01	(1.09,1.06,1.06)	1.00
	(−2,−2,−2)	2.05	(1.17,1.12,1.12)	0.99
	(−5,−5,−5)	2.30	(1.42,1.30,1.29)	0.96

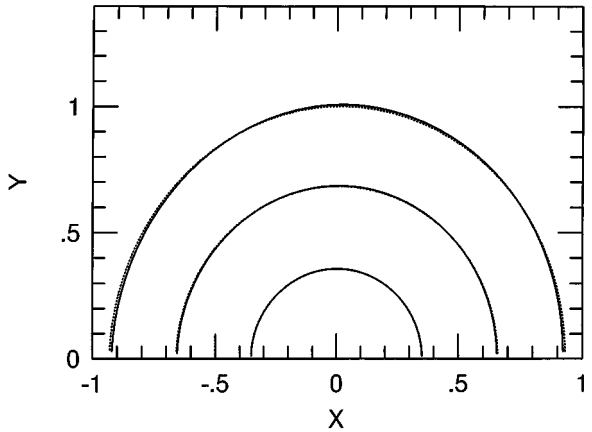

FIG. 6. Location of the AH in $\theta=\pi/8$ (inner lines), $\pi/4$ (middle lines), and the equatorial planes (outer lines) for case (e) of the time-asymmetric 3D hypersurface ($\sigma=\omega=5$). Solid lines denote the result when we give K_{ij} analytically, and dotted lines denote that when K_{ij} is obtained from numerical calculation.

$I(\infty)/16\pi M_0 = 0.1$, we need to take grids at least up to $L \sim 5$ to reduce the estimation error of M within $\sim 1\%$, and for the case $I(\infty)/16\pi M_0 = 0.2$, we need $L \sim 6$. Furthermore, with an increase of $I(\infty)$, we need to take large L to keep the error within $\sim 1\%$. On the other hand, we want to take a finer grid to avoid (I) as well as to solve Eq. (3.1) with a sufficient accuracy, but it is restricted due to (II) and a restricted grid number. Thus, an error of $\sim 1-2\,\%$ is unavoidable unless we take a larger number of grid or we perform the integral in a more sophisticated manner [19]. However, the purpose of this paper is not to present the highly accurate results for ψ, M, and $A_{\rm AH}$, but to demonstrate that the AH finder works well. For this purpose, the above accuracy seems enough. Hence, we do not pursue improving accuracy any longer in this paper.

To determine the AH from Eq. (2.6), $\psi(h,\theta,\varphi)$ is needed. So, we calculate it by interpolation from numerical data sets of $\psi(x_i, y_j, z_k)$ which is assigned only at discrete grid points. As a trial function of $h(\theta,\varphi)$, we give $h(\theta,\varphi)=1$. In all cases, the AH is determined within a small fraction of a grid zone in ~ 10 iterations.

In Table III, we show the area, the intersection of the two-surface of the AH with x, y, and z axes, and the gravitational mass in the time-asymmetric 3D hypersurface. The results described here are calculated when we adopt the homogeneous grid with $\delta x = \delta y = \delta z = 0.09$. As mentioned above, each value will have the error of $\sim 1-2\,\%$. From Table III, we soon recognize the following facts.

(1) Because of the purely collapsing motion of matter [cases (a) and (d)], the coordinate radius of the AH becomes larger, while the expanding motion acts oppositely.

(2) In the case where the matter is purely collapsing or expanding [cases (a) and (d)], the area of the AH is approximately $16\pi M^2$. Hence, in this case, even if we start a numerical simulation from such an initial data, gravitational radiation is hardly emitted. On the other hand, if the matter has a rotation or shear motion [cases (b) and (c)], the area is sufficiently less than $16\pi M^2$. So that, if we start a simulation from these initial data sets, gravitational radiation may be emitted.

Feature (1) is qualitatively consistent with previous works performed in the axisymmetric cases [20,21,18]. Also, a previous work [20] showed that in the case when the BH has the angular momentum, the area of the AH is always smaller than $16\pi M^2$. Hence, the results obtained here seem reliable.

Finally, to demonstrate that the present method works well even in the case when we obtain K_{ij} numerically, we solve the equations for B_i and χ, as well as that for ψ in the case (e) of $\sigma = \omega = 5$ as an example. To solve the Poisson equations for B_i, χ, and ψ, we use the homogeneous grid of $\delta x = 0.09$ with a grid number of (101,101,51). Since we numerically obtain K_{ij}, not only $\psi(h,\theta,\varphi)$, but also $K_{ij}(h,\theta,\varphi)$ must be calculated by interpolation from those assigned only at discrete grid points in determining the AH from Eq. (2.6). In Fig. 6, we show the location of the AH in $\theta = \pi/8$ (inner lines), $\pi/4$ (middle lines), and the equatorial planes (outer lines) for two cases; one is the case where K_{ij} is analytically obtained (solid line) and the other is the case where K_{ij} is numerically calculated (dotted line). It is found that the location of the AH in the two cases agrees within a small fraction of a grid zone. Also, the areas agree with each other within 0.5%. Thus, the present method is expected to work well even for fully numerical data sets of 3D hypersurfaces.

VI. SUMMARY

In this paper, we have described a method to determine the AH on a special family of 3D hypersurfaces which has π-rotation symmetry around the z axis as well as the reflection one with respect to the equatorial plane. In the present method, we solve the 2D elliptic-type equation for the AH as the boundary value problem in contrast with a previous work [6]. To check whether the method works well, we have applied the 3D AH finder not only to data sets of time-symmetric 3D hypersurfaces which are given analytically, but also to that of time-asymmetric 3D hypersurfaces obtained numerically. In all cases, we found that the 3D AH finder brought accurate results. Hence, we expect that it is also useful to determine the AH for a wide variety of formation problems of BH in numerical relativity such as coalescence of BNS's of equal mass to be a BH [11], collapse of a rotating ellipsoid to be a BH, collapse of quadrupole gravitational waves to be a BH [22], and so on. We will apply the present method to determine the AH in such numerical simulations in the near future.

ACKNOWLEDGMENTS

The author would like to thank K. Nakao for frequent useful discussions and for helpful comments on this manuscript, and T. Nakamura for useful discussions. Numerical computations were performed on YHP-715 workstations. This work was, in part, supported by a Grant-in-Aid for Creative Basic Research of Ministry of Education, Culture, Science and Sports, No. 08NP0801.

APPENDIX

Here, we briefly describe how to make the numerical code to determine the AH when the 3D hypersurfaces has the reflection symmetries with respect to x-y, y-z, and z-x planes. Such an AH finder will be useful in investigating the formation process of BH's in the triaxial systems such as collapse of the triaxial ellipsoid. In the case when such symmetries exist, we take a grid which covers $0 < \varphi < \pi/2$ and $0 < \theta < \pi/2$. The boundary conditions at $\theta = 0$ and $\pi/2$ are the same as that for the case of the π-rotation symmetry, but the boundary conditions at $\varphi = 0$ and $\pi/2$ change to the reflection symmetric boundary conditions and the finite differences there (i.e., at $j = 1$ and N_φ) become

$$h_{,\varphi\varphi} = \frac{h_{2,j} - h_{1,j}}{\delta\varphi^2}, \quad h_{,\varphi\varphi} = \frac{-h_{N_\varphi,j} + h_{N_\varphi - 1,j}}{\delta\varphi^2}. \qquad \text{(A1)}$$

Thus, the schematic form of M_{ij} becomes

$$M_{ij}=\begin{pmatrix}
* & * & & & * & & & & & & & & \\
 & * & * & & & * & & & & & & & \\
 & * & * & * & & & * & & & & & & \\
 & & * & * & * & & & * & & & & & \\
 & & & * & * & & & & * & & & & \\
 & & & & & * & * & & & * & & & \\
 & * & & & & * & * & * & & & * & & \\
 & & * & & & & * & * & * & & & * & \\
 & & & * & & & & * & * & * & & & * \\
 & & & & * & & & & * & * & & & \\
 & & & & & * & & & & * & * & * & \\
 & & & & & & * & & & & * & * & * \\
 & & & & & & & * & & & & * & * \\
 & & & & & & & & * & & & & *
\end{pmatrix}. \tag{A2}$$

In this case, M_{ij} has only five diagonal components, so that the matrix equation can be also solved by the ILUCGS method [9] as mentioned in Sec. II.

[1] A. Abramovici *et al.*, Science **256**, 325 (1992); K. S. Thorne, in *Proceedings of the 8th Nishinomiya-Yukawa Memorial Symposium on Relativistic Cosmology*, edited by M. Sasaki (Universal Academy Press, Tokyo, 1994), p. 67.

[2] C. Bradaschia *et al.*, Nucl. Instrum. Methods Phys. Res. A **289**, 518 (1990).

[3] S. W. Hawking and G. F. R. Ellis, *The Large Scale Structure of Space-time* (Cambridge University Press, Cambridge, England, 1973).

[4] S. Hughes, C. R. KeetonII, P. Walker, K. Walsh, S. L. Shapiro, and S. A. Teukolsky, Phys. Rev. D **49**, 4004 (1994).

[5] J. Libson, J. Masso, E. Seidel, W-M. Suen, and P. Walker, Phys. Rev. D **53**, 4335 (1996).

[6] T. Nakamura, K. Oohara, and Y. Kojima, Prog. Theor. Phys. Suppl. **90**, 21 (1987).

[7] K. Nakao (private communication).

[8] J. Libson, J. Masso, E. Seidel, and W.-M. Suen, in *General Relativity*, Proceedings of the 7th Marrl Grossmann Meeting, Stanford, California, 1994, edited by R. Ruffini and M. Keiser (World Scientific, Singapore, 1995), Report No. gr-qc/9412058 (unpublished).

[9] K. Murata, M. Natori, and Y. Karaki, *Large-Scale Numerical Simulation* (Iwanami, Tokyo, 1990).

[10] For example, J. W. York, Jr., in *Source of Gravitational Radiation*, edited by L. L. Smarr (Cambridge University Press, Cambridge, England, 1979), p. 83.

[11] T. Nakamura, in *Proceedings of the 8th Nishinomiya-Yukawa Memorial Symposium on Relativistic Cosmology* [1], p. 155.

[12] J. R. Wilson, G. J. Mathews, and P. Marrobetti, Phys. Rev. D **54**, 1317 (1996).

[13] C. W. Misner and J. A. Wheeler, Ann. Phys. (N.Y.) **2**, 525 (1957).

[14] D. R. Brill and R. W. Lindquist, Phys. Rev. **131**, 471 (1963).

[15] A. M. Abrahams, K. R. Heiderich, S. L. Shapiro and S. A. Teukolsky, Phys. Rev. D **46**, 2452 (1992).

[16] A. Cadez, Ann. Phys. (N.Y.) **83**, 449 (1974).

[17] N. T. Bishop, Gen. Relativ. Gravit. **14**, 717 (1982).

[18] G. B. Cook and A. M. Abrahams, Phys. Rev. D **46**, 702 (1992).

[19] G. B. Cook, M. W. Choptuik, M. R. Dubal, S. Klasky, R. A. Matzner, and S. R. Oliveira, Phys. Rev. D **47**, 1471 (1993); G. B. Cook, *ibid.* **50**, 5025 (1994).

[20] G. B. Cook and J. W. York, Jr., Phys. Rev. D **41**, 1077 (1990).

[21] A. M. Abrahams and G. B. Cook, Phys. Rev. D **50**, R2364 (1994).

[22] M. Shibata and T. Nakamura, Phys. Rev. D **52**, 5428 (1995).